Design of a Dual-Linearly Polarized Endfire Antenna

Weiquan Zhang, Yue Li, *Senior Member, IEEE*, and Zhijun Zhang, *Fellow, IEEE*

***Abstract*— In this article, a dual-linearly polarized endfire antenna is proposed with high gain and stable radiation patterns. A double-sided slot array antenna (DSSAA) and a corrugated rectangular metal strip (CRMS) are employed to realize vertical and horizontal polarization (HP), respectively. Omnidirectional radiation pattern is obtained by etching transverse slots on both sides of the top and bottom metallic plates of a cavity. Based on the double-sided slot antenna, a DSSAA is proposed and fed by an air-substrate parallel strip line (PSL) for stable endfire radiation patterns. Then, the top plate of the DSSAA is reused as a CRMS for HP and compact size. To verify this concept, an all-metal prototype was fabricated and measured. Both the simulation and experimental results show that the DSSAA and the CRMS could offer the highest endfire gains of 12.5 and 12.9 dB, respectively, within a footprint of $3.47\lambda_0 \times 0.72\lambda_0 \times 0.13\lambda_0$ (λ_0 is the free-space wavelength at the center frequency). Moreover, an overlapping bandwidth of 7.6% is realized with $|S_{11}| < -10$ dB, gain variation less than 3 dB. This work may provide useful references for designing dual-polarized endfire antennas with stable radiation patterns, high gain, and compact size.**

***Index Terms*— Dual-linear polarization, endfire antenna, high endfire gain.**

I. Introduction

ENDFIRE antennas have received great attention for long-distance directional communications since they enable efficient data rates and high-quality reception. To realize endfire beam, one approach is to use Yagi-Uda [1]–[8] and log-periodic antennas [9]–[15]. A microstrip Yagi array antenna with endfire radiation and vertical polarization (VP) was realized in [7]. The radiation beams in [7] and [8] are not exactly endfire due to the tilted radiation patterns of the radiation elements and the impact of the finite ground plane. In [9], a log-periodic monopole array antenna was proposed for endfire radiation with VP. A compact-printed log-periodic dipole array antenna in [14] was designed for radiating horizontal polarization (HP) wave in the endfire direction. It is noted that the realized endfire gain of log-periodic antennas is limited due to the partly radiated property.

On the other hand, many leaky-wave antennas are explored for endfire radiation. By properly adjusting the energy-leak rate along a leaky-wave antenna, a large and uniform radiating aperture can be obtained for high gain [16]. Leaky-wave antennas with large radiating aperture were fed by substrate integrated waveguide [17]–[19] or air-substrate transmission line [20]–[23]. In [21], a slot array antenna was fed by microstrip line. An endfire beam was realized since the TEM mode provides a proper phase constant in [21]. Recently, many traveling-wave antennas based on spoof surface plasmon polaritons (SSPPs) transmission lines were investigated to realize endfire radiation with HP [24]–[27]. In [24], an endfire radiating planar prototype of a corrugated rectangular metal strip (CRMS) was proposed with high endfire gain and wide bandwidth.

Polarization diversity is widely used in radar, imaging, and wireless communication systems. Multipolarized antennas were widely exploited to enhance the channel capacity and solve the polarization mismatch issues [28], [29]. Dual-polarization and endfire radiation can be achieved by using a log-periodic dipole array or a Yagi antenna [30]–[32]. In [30], a vertically stacked Yagi antenna was proposed for dual-polarization with a size of $0.96\lambda_0 \times 0.96\lambda_0 \times 1.16\lambda_0$ and an operating bandwidth of 4%. A wideband nonplanar log-periodic dipole array was designed for endfire radiation with a size of $3.28\lambda_0 \times 2.96\lambda_0 \times 2.96\lambda_0$ and an average gain of 6.7 dB within the working bandwidth. Besides, Vivaldi and horn antennas are also capable of realizing dual-polarized endfire radiation at the expense of large transverse size [33], [34]. Therefore, it is still a challenge to achieve a dual-linearly polarized endfire antenna with high gain and compact size.

In this article, a dual-linearly polarized antenna is realized by combining two different types of endfire antennas. An endfire slot array antenna with VP is realized by etching transverse slots on both top and bottom sides of a rectangular waveguide. Besides, the double-sided slot array antenna (DSSAA) is fed by a TEM-guided wave parallel strip line (PSL) with air media. Hence, stable endfire radiation patterns with high gain can be obtained. Moreover, to realize horizontal-polarized endfire radiation, the top layer of the DSSAA also works as a CRMS for low profile. Hence, the polarization-flexible functionality is obtained by combining the two antennas with orthogonal linear polarization excited by different inputs. A prototype was fabricated to provide experimental verification of the idea. The measured highest endfire gains are 12.5 and 12.9 dB for the HP and VP, respectively, within a footprint of $3.47\lambda_0 \times 0.72\lambda_0 \times 0.13\lambda_0$.

The main contribution of this work can be summarized as follows.

1) An air-substrate PSL is applied here to feed a DSSAA for steady endfire radiation. Moreover, the proposed

Manuscript received December 16, 2020; revised May 11, 2021; accepted May 25, 2021. Date of publication June 25, 2021; date of current version December 16, 2021. This work was supported by the National Natural Science Foundation of China under Contract 61971254. *(Corresponding author: Zhijun Zhang.)*

The authors are with the Department of Electronic Engineering, Tsinghua University, Beijing 100084, China, and also with the Beijing National Research Center for Information Science and Technology, Tsinghua University, Beijing 100084, China (e-mail: zjzh@tsinghua.edu.cn).

Color versions of one or more figures in this article are available at https://doi.org/10.1109/TAP.2021.3090842.

Digital Object Identifier 10.1109/TAP.2021.3090842

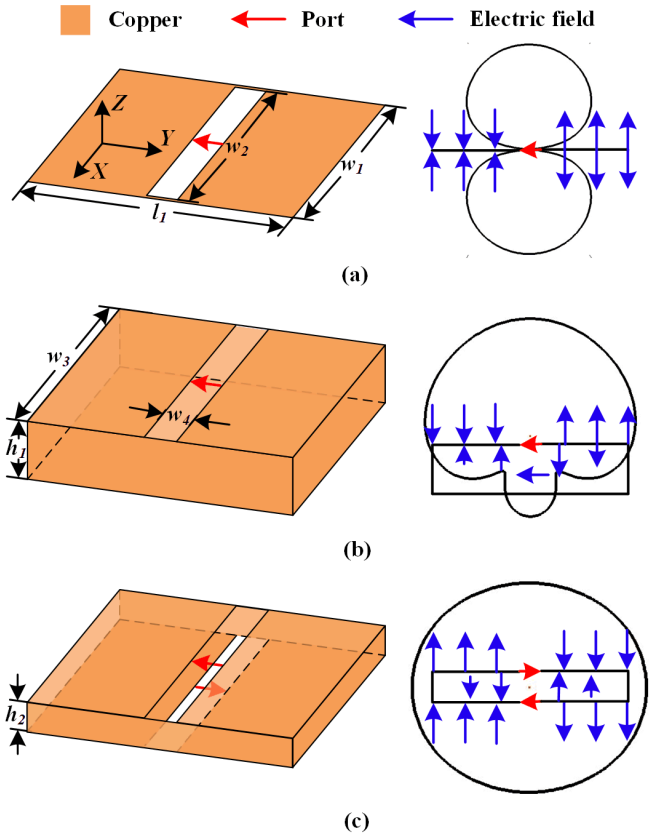

Fig. 1. Schematics of the radiation patterns and E-field distributions with different vertically polarized radiation elements at 4 GHz in the E-plane (YZ plane). (a) Planar slot antenna. (b) Cavity-backed slot antenna. (c) Double-sided slot antenna.

vertically polarized structure has the advantage of high gain and an acceptable profile.

2) Compact size is achieved by designing the top layer of the DSSAA as an antenna with HP.
3) High endifre gains are realized in two polarization states.

The remainder of this article is organized as follows. In Section II, the basic radiating structure and the operation mechanism are presented and discussed. The structure and parametric studies of the proposed antenna are presented in Section III. In Section IV, the antenna fabrication, simulated, and measured performance of the antenna are provided. Finally, Section V summarizes our work.

II. Antenna Design

A. Vertical-Polarization Endfire Antenna

To realize an endfire array antenna, an antenna element with an omnidirectional radiation pattern is desirable according to the pattern multiplication theory [35]. Fig. 1 presents the schematic of the radiation patterns and E-field distributions with different vertically polarized radiation elements. The detailed dimensions are listed in Table I. As shown in Fig. 1(a), the undesirable pattern null can be seen in the endfire ($+Y$) direction for the planar slot antenna. Hence, endfire array radiation patterns are unrealizable based on the planar slot antenna.

TABLE I
Detailed Dimension of the Different Antennas

Parameter	Value(mm)	Parameter	Value(mm)
l_1	40	w_4	5.5
w_1	32.5	h_1	20
w_2	32	h_2	10
w_3	32		

The cavity-backed slot antenna with a tilted radiation pattern has the potential to be used as the basic radiation element of an endfire array antenna but cannot reach exactly endfire radiation, as shown in Fig. 1(b). Besides, the radiation capacity of the cavity-backed slot element becomes worse with the decrease of the profile since parallel electric fields cannot exist on the surface of the metal plate. Hence, the profile of the cavity-backed slot antenna was selected as $0.26\lambda_0$ in [21] for effective radiation. Hence, to realize exactly endfire radiation without beam tilting and high profile, a double-sided slot element with vertically polarized omnidirectional radiation pattern is employed here as illustrated in Fig. 1(c). It is noted that the slots on the top and bottom plates should be excited with equal amplitude and inverse phase so as to obtain the omnidirectional radiation pattern.

A SIW leaky-wave antenna with double-sided slots on the top and bottom planes is presented in [18]. However, the beam direction was sensitive to the frequency since the dispersive TE_{10} mode was excited in the SIW. To address this issue, a different feeding method is used in this article. A TEM-guided wave PSL is adopted to feed the double-sided slot antenna as shown in Fig. 2(a). The vector electric distribution is plotted in Fig. 2(b). Since the central line of the PSL is aligned at the location of the maximum electric fields of the slot antenna, the E-coupling occurs, and the radiating element radiates vertically polarized wave. An omnidirectional radiation pattern can be obtained since the slots on the top and bottom metallic plates are effectively excited with equal amplitude and inverse phase as shown in Fig. 2(b). Based on the proposed radiating element in Fig. 2(a), a DSAA fed by an air-substrate PSL is proposed, as shown in Fig. 3. Stable endfire radiation patterns are obtained since the feeding structure works on the TEM mode. Hence, the TE_{10} mode of the rectangular waveguide is undesired. To suppress the TE_{10} mode, the width of the waveguide is reduced. The w_3 is optimized as 0.43λ (λ is the free-space wavelength at 4 GHz) for increasing the suppression of the TE_{10} mode. The cutoff frequency of the TE_{10} mode is about 4.6 GHz with $w_3 = 0.43\lambda$. The spacing between two adjacent slots is designed to be about $0.25\lambda_0$ since the energy reflected from two adjacent radiating elements can cancel each other out. It is noted that compared with the Yagi-Uda and log-periodic antennas, the series-feed DSSAA has the ability to realize a long structure with high endfire gain since the coupling energy of each radiating element of the proposed antenna could be designed.

B. HP Endfire Antenna

HP endfire antenna with high gain can be realized by exciting the surface-wave mode (TE_1 mode) in a metal strip [24],

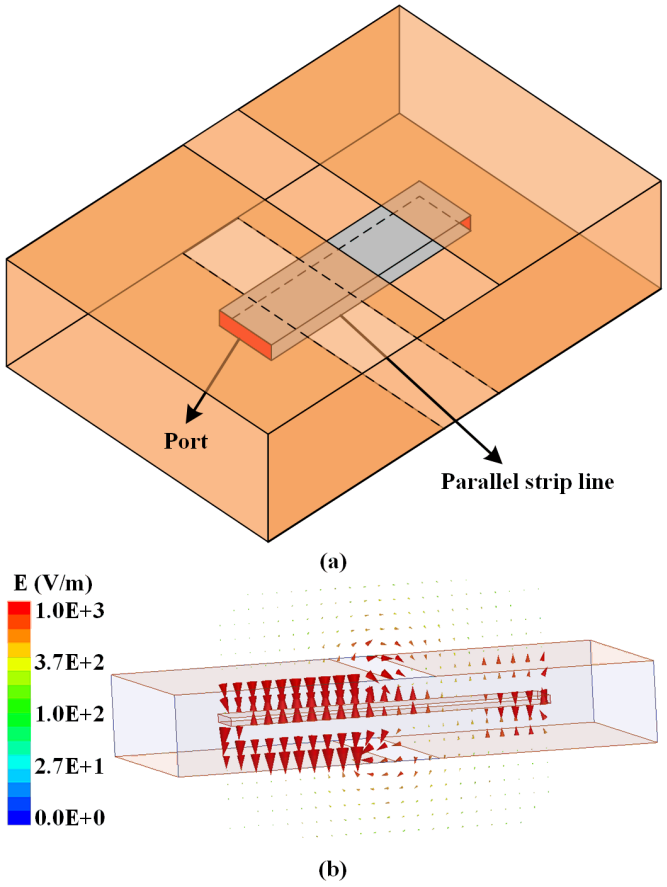

Fig. 2. (a) Proposed vertically polarized radiation antenna element with feeding structure. (b) Vector E-field distribution of the double sides slot antenna element at 4 GHz.

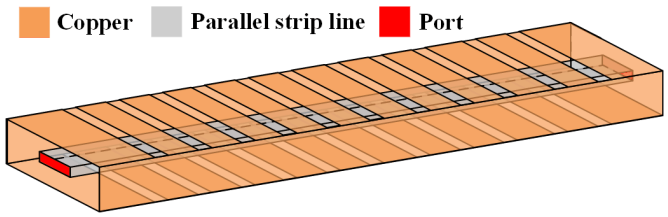

Fig. 3. Configuration of the DSAA fed by an air-substrate PSL.

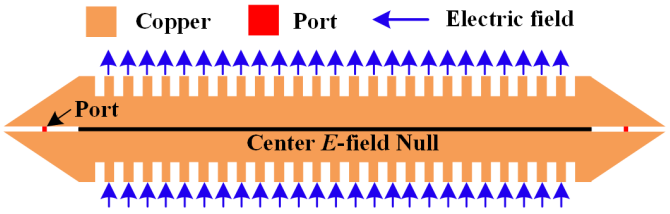

Fig. 4. Geometry of the CRMS and schematic of the vector E-field distribution of the TE1 mode.

as shown in Fig. 4. Periodic grooves are etched on both edges of the metal strip to tailor the phase constant and leak rate for high endfire gain. The CRMS is fed by magnetic excitation. Two taper transitions are implemented at both sides of the antenna to realize better impedance match. Besides, a center E-field null is obtained of the TE_1 mode as shown in Fig. 4.

TABLE II
DETAILED DIMENSION OF THE PROPOSED ANTENNA

Parameter	Value(mm)	Parameter	Value(mm)
L	220	l_2	15
W	55	P_1	18
P	8.5	L_{taper}	22
H	8	w_1	1
a	4.3	w_2	5.5
h	1	w_3	6.5
h_1	10	w_4	80
h_2	4.5	w_5	40.5
l_1	32	g	2

Based on the analysis mentioned above, a dual-linearly polarized antenna can be realized by properly combining the two distinct radiation structures without deteriorating their radiation patterns and occupying a large space.

III. ANTENNA STRUCTURE AND SIMULATION RESULTS

A. Antenna Structure

Based on the antennas in Figs. 3 and 4, a dual-linearly polarized antenna is proposed, as shown in Fig. 5. Three metal sheets and two metal strips are used here. Fig. 5(a) depicts the top plate of the antenna. The top plate of DSSAA is reused as the CRMS. The PSL is composed of two metal strips with air substrate as shown in Fig. 5(b). One metal sheet is bent to form the side plates and bottom plate with several slots etched. Hence, the DSSAA is implemented by combining the top and bottom metal sheets and fed by the TEM-guided wave PSL. The length of the bottom and top plates of the antenna is $2.9\lambda_0$ and $3.5\lambda_0$, respectively. The proposed antenna is shown in Fig. 5(c). A square reflector is loaded behind to suppress the backside radiation caused by the feed radiation of the CRMS. The distance between the CRMS and the reflector is defined by parameter g, which can be used for impedance bandwidth improvement. The CRMS is fed through Port 1 by the magnetic excitation, while other ports are matched by 50 Ω to absorb the residual power. And the DSSAA is fed through Port 3 while other ports are matched by 50 Ω. The whole dimension of the proposed antenna is $3.47\lambda_0 \times 0.72\lambda_0 \times 0.13\lambda_0$ at 3.95 GHz. The parameters are optimized in full-wave simulation software HFSS [36] and the detailed dimensions are given in Table II. In order to highlight the novelty of this work, a comparison between this work and the proposed antennas in [21] and [24] is given as follows.

1) Cavity-backed slot element was utilized in [21] for endfire radiation with high profile ($0.26\lambda_0$) and tilted radiation patterns. Since a double-sided slot element is applied in this work, low-profile ($0.13\lambda_0$) and stable endfire radiation are obtained. Therefore, the proposed vertically polarized antenna has different radiating elements with a lower profile and exactly endfire radiation.
2) Microstrip line and PSL are applied as feeding structures in [21] and this work, respectively. PSL is used to feed a double-sided slot array for the first time.

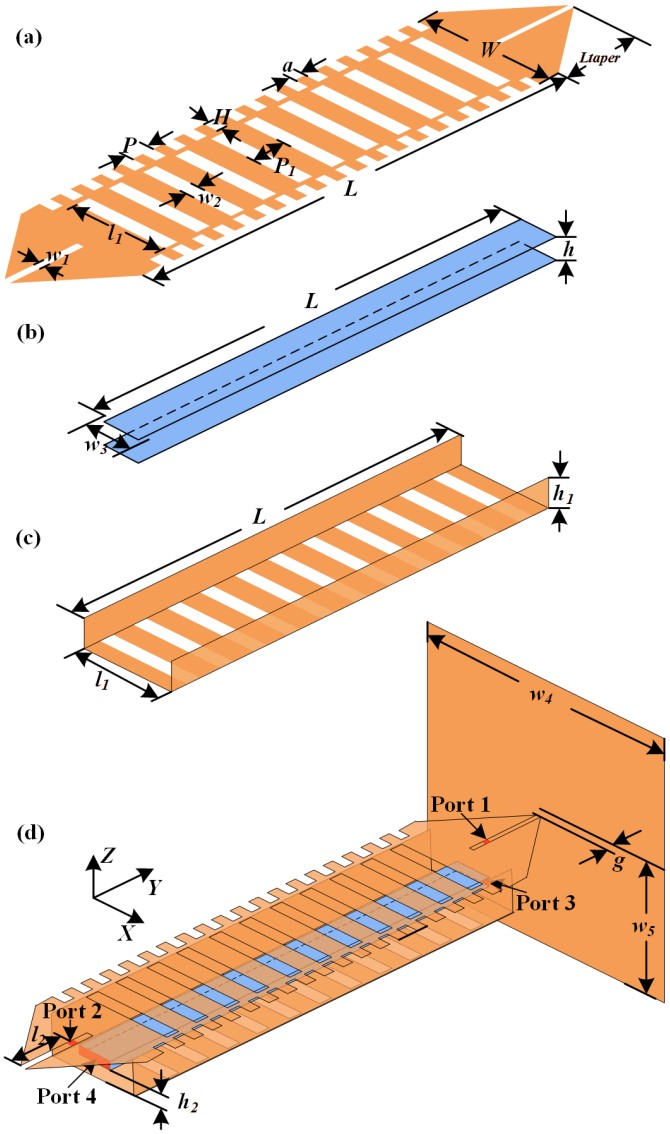

Fig. 5. Configuration of the dual-polarized antenna. (a) Top plate of the antenna. (b) Feeding structure of the DSSAA. (c) Bottom and side plates of the antenna. (d) Perspective view of the proposed antenna.

3) Both the antennas in [21] and [24] are single-polarized. By skillfully reusing the top layer of the DSSAA as a horizontally polarized endfire antenna, compact size and dual-polarization are realized in this work.

B. Dispersion Analysis and Radiation Performance

To further reveal the radiation principle, the normalized phase constant β/k_0 and leakage rate α/k_0 verse the frequency are presented in Fig. 6. For the MRSA, the surface-wave mode is the dominant mode. Hence, the phase constant is obtained from the E-field distributions of the surface wave. Since the energy of the surface-wave mode focus on the top and bottom surfaces of the DSSAA, the phase constant is sampled from the position right above the top plate. To make an intuitive comparison, the phase constants in free space, of the theoretical Hansen–Woodyard (H–W) condition [37] are also shown here. The optimum phase constant was proposed by Hansen–Woodyard [37] for maximum endfire directivity

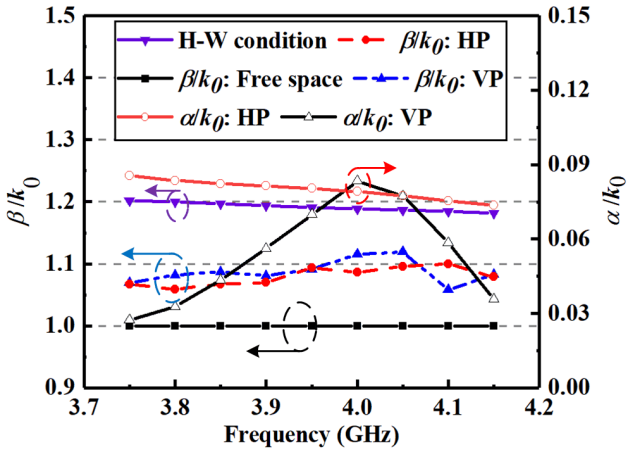

Fig. 6. Simulated normalized phase constant β/k_0 and leak rate α/k_0 versus frequency.

based on the basic premise of a finite continuous line source with a uniform amplitude distribution. It is noted that leak rate α was not considered in [37]. Hence, the H–W condition does not necessarily yield the maximum possible endfire gain since the leak rate is not taken into consideration. During the antenna design, an appropriate leak rate is desired for uniform E-field magnitude distribution along the antenna and ensuring that most of the power is radiated. Therefore, high endfire gain can be obtained with the β/k_0 closing to the H–W condition and appropriate leak rate. As shown in Fig. 6, the DSSAA and the CRMS have similar and stable β/k_0 within the operating bandwidth from 3.75 to 4.15 GHz. The leak rate is decreased with the increase of β/k_0 since more fields are confined in the surface with the increase of β/k_0. Hence, β/k_0 of the DSSAA and CRMS are smaller than H–W condition for obtaining an appropriate leak rate. Though TEM mode is excited in the PSL, the actual propagation mode is affected by the radiating double-sided slots. Hence, the phase constant of DSSAA is perturbed to some extent. It can be seen that the leak rate of the CRMS is decreasing gradually with the frequency increasing. However, the leakage rate of the DSSAA changes obviously within the operating bandwidth since the coupling between the double-sided slots and the PSL is related to frequency. High leakage rate of the DSSAA is obtained when the slots are strongly resonant.

The E-field distribution of the CRMS at 4 GHz is depicted in Fig. 7 with Port 1 excited. Fig. 7(a) illustrates the E-field amplitude distribution in the YZ plane. A uniform E-field distribution along the Y-axis is seen due to the surface-wave transmission. The absolute E-field intensity along the reference line (shown in the inset) is also given in Fig. 7(b) to demonstrate the uniformity of the E-fields.

The E-field distribution of the DSSAA at 4 GHz is shown in Fig. 8 with Port 3 excited. It is found that all the slot antennas contribute to the radiation. High endfire gain can be obtained due to the uniformity of the E-fields.

C. Parameter Analysis

The value of the H is a vital factor to adjust the phase constant and leak rate of the CRMS. Fig. 9 shows the

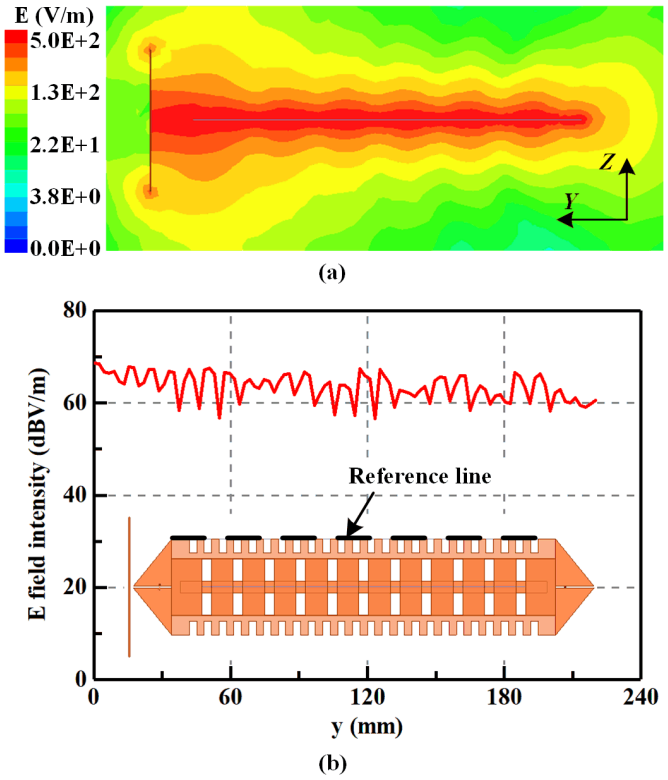

Fig. 7. Simulated E-field distribution at 4 GHz when Port 1 is excited. (a) Complex E-field amplitude distribution in the YZ plane. (b) E-field intensity along the reference line shown in the inset.

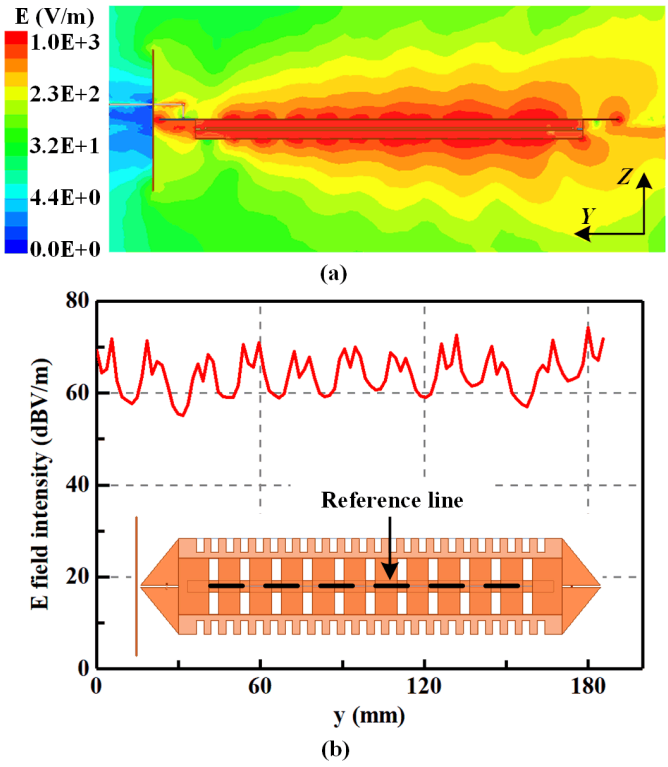

Fig. 8. Simulated E-field distribution at 4 GHz when Port 3 is excited. (a) Complex E-field amplitude distribution in the YZ plane. (b) E-field intensity along the reference line shown in the inset.

simulated radiation patterns of the CRMS with the value H varied from 5 to 11 mm with 3 mm step in the range. The phase constant increases with the increase of H. To realize a higher endfire gain, $H = 8$ mm is selected finally.

The effect of the parameter l_1 on $|S_{33}|$ and $|S_{43}|$ is shown in Fig. 10, by varying it from 30 to 34 mm with 2 mm step in the range. The value of the l_1 is a key parameter to adjust the operating frequency of the DSSAA. The resonant frequency of the double-sided slots shifts downward with l_1 increasing due to the increase of the resonant length of the double-sided slots. Effective radiation is realized as long as most of the energy in the PSL is coupled into the DSSAA. Therefore, the value of l_1 has a great effect on the DSSAA. For the CRMS, as l_1 increases, the simulated $|S_{11}|$ and $|S_{21}|$ are almost unaffected. The results are not given here for brevity. This phenomenon is corresponding to the electric field distribution of the CRMS as shown in Fig. 4. A center E-field null of the TE_1 mode is obtained while a center-strong E-field is obtained for the DSSAA. To cover the desired frequency range, $l_1 = 32$ mm is selected finally.

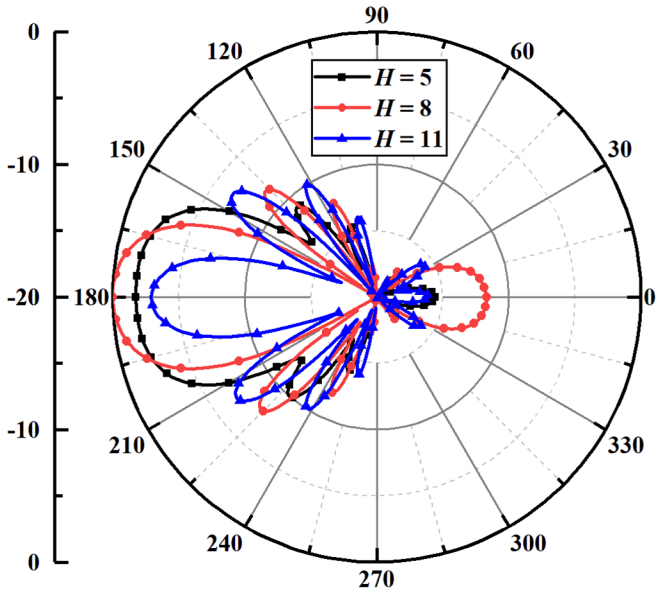

Fig. 9. Simulated normalized radiation patterns of the CRMS with different H in the YZ plane.

IV. Experimental Verification

A. Antenna Fabrication

The proposed dual-polarized antenna was fabricated and measured to provide a verification of the approach. The prototype is shown in Fig. 11. The antenna is composed of three copper sheets, two copper strips, and four 50 Ω coaxial cables. The 50 Ω matched loads were connected at other ports to absorb the residual power when one port was excited by a coaxial cable. For a clearer view, the coaxial cables and welds of Port 1 and Port 3 were enlarged. The two coaxial cables passed through the square reflector, feeding the antenna. The CRMS was fed through Port 1 by a 50 Ω semirigid cable with

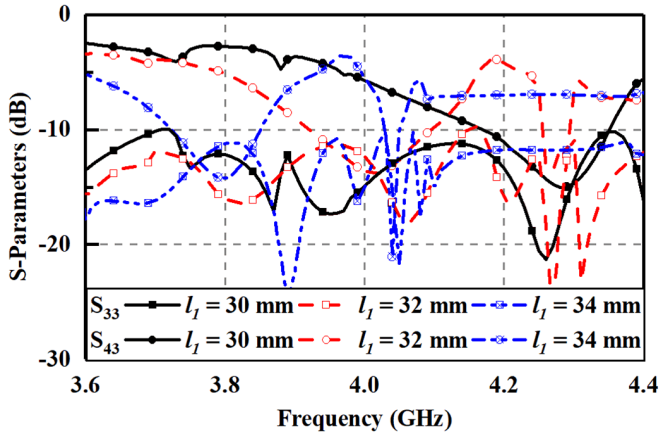

Fig. 10. Variation of the resonant frequency of the DSSAA with respect to length l_1.

outer conductor soldered at one side of the feeding slot and inner conductor soldered at another side. In the same way, a 50 Ω semirigid cable was used for feeding the DSSAA with outer conductor soldered at the lower copper strip and inner conductor soldered at another strip. The metals were manufactured by 0.5 mm-thick brass plates ($\sigma = 1.5 \times 10^7$ S/m) with laser cutting process. One of the copper sheets with 15 slots notched was bent to form the side plates and the bottom plate of the antenna. And one of the coppers is recognized as the reflective plate. Since the PSL was located in the middle of the DSSAA, some polyvinyl chloride (PVC) foams with a thickness of 4 mm under the PSL were used as supports, as shown in Fig. 11(a). The real part of the relative permittivity of the PVC foam is around 1.21. Besides, some PVC foams with a thickness of 1 mm were placed between the two metal strips since the weight of the strips is too light to ensure the stability of the transmission line. Using as few foams as possible to avoid deteriorating the performance of the DSSAA. S-parameters of the antenna were measured using a N5071B vector network analyzer (300 kHz–9 GHz). And the gains and radiation patterns were measured in a far-field anechoic chamber.

B. S-Parameters

Fig. 12 shows the measured and simulated S-parameters. It can be seen that the measured data agree well with the simulated results. A little shift of the operating frequency of the DSSAA occurs for the measured data compared to the simulated results. The discrepancy between the measurement and simulation is mainly caused by the foams loaded. The reflection coefficients are below −10 dB in 3.8–4.1 GHz band in two polarization states.

C. Radiation Performance

The measured and simulated normalized radiation patterns of the fabricated prototypes at 4 GHz are shown in Fig. 13 with good agreement between simulation and measurement. From these results, it is clear that stable endfire radiation patterns in two polarization states are achieved. The measured half-power beamwidths of the CRMS and the DSSAA at 4 GHz are 20° and 35° in the E-plane and 28° and 35° in the H-plane, respectively. Therefore, a dual-linearly polarized antenna with stable endfire radiation patterns is realized.

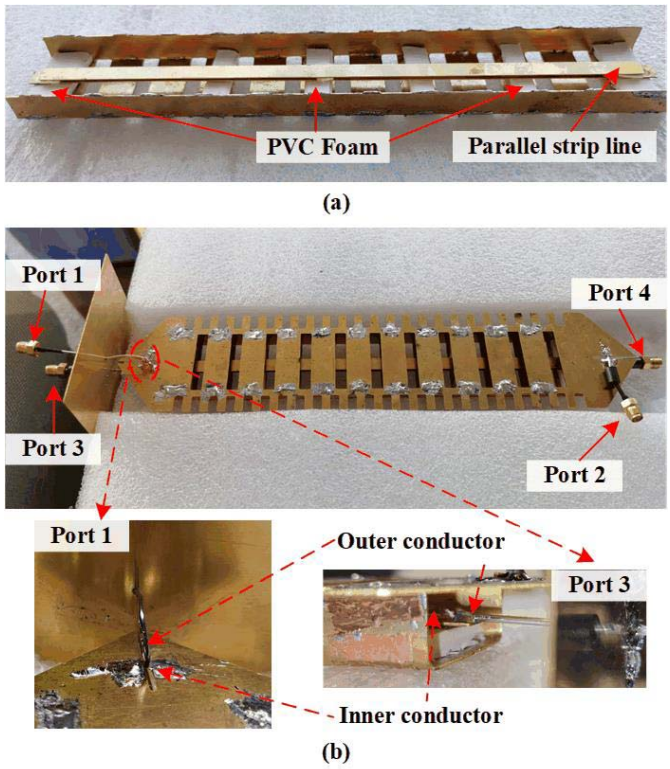

Fig. 11. Fabricated prototype of the proposed antenna. (a) Feeding structure of the DSSAA. (b) Whole proposed antenna.

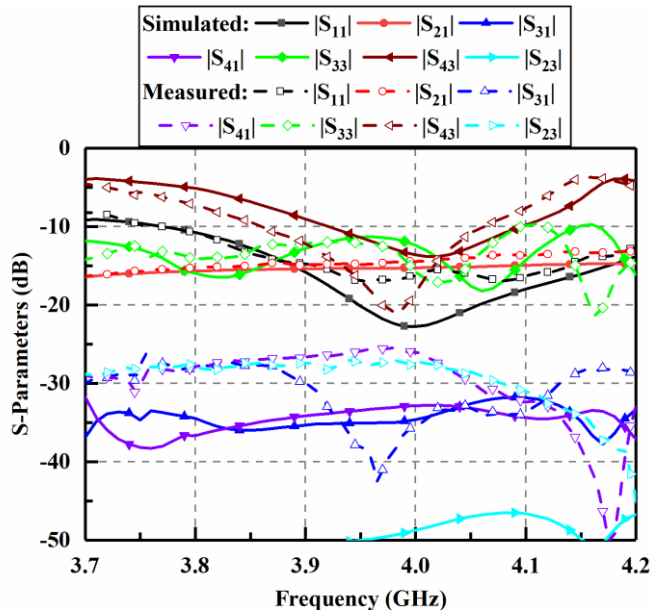

Fig. 12. Simulated and measured S-parameters of the proposed antenna.

TABLE III
COMPARISON AMONG THE ENDFIRE ANTENNAS (NG: NOT GIVEN)

Reference	Polarization	Length (λ_0)	Width (λ_0)	Height (λ_0)	Bandwidth (%)	Max. Endfire Gain (dBi)	3 dB Endfire Gain BW (%)
[7]	VP	3.43	1.715	0.03	11.7	10.4	11.7
[12]	VP	5.8	2	0.16	80.3	6	NG
[21]	VP	3.50	0.43	0.26	8.4	11.8	8.4
[24]	HP	3.0	0.49	/	40.0	14.2	27.7
[25]	HP	2.85	0.32	/	12.5	9.2	12.5
[26]	HP	1.36	0.86	/	70.3	8.6	NG
[31]	HP & VP	1.16	0.96	0.96	4	9.76	NG
[32]	HP & VP	3.28	2.96	2.96	178.9	< 8	178.9
[33]	HP & VP	3.2	2.93	2.93	166.0	11.2	NG
Our Work	HP & VP	3.47	0.72	0.13	HP: 20.3 VP: 7.6	HP: 12.5 VP: 12.9	HP: 7.6 VP: 7.6

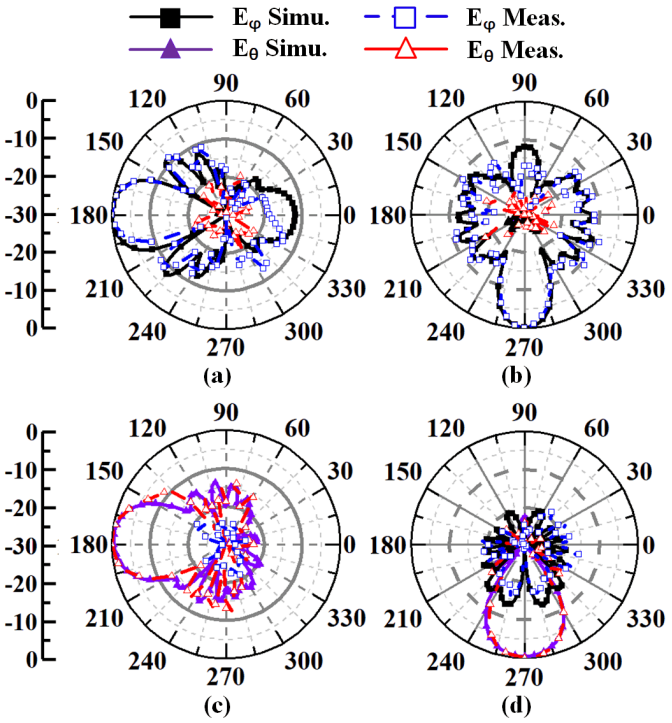

Fig. 13. Simulated and measured normalized radiation patterns of the proposed antenna at 4 GHz. (a) Port 1 in the *YZ* plane. (b) Port 1 in the *XY* plane. (c) Port 3 in the *YZ* plane. (b) Port 3 in the *XY* plane.

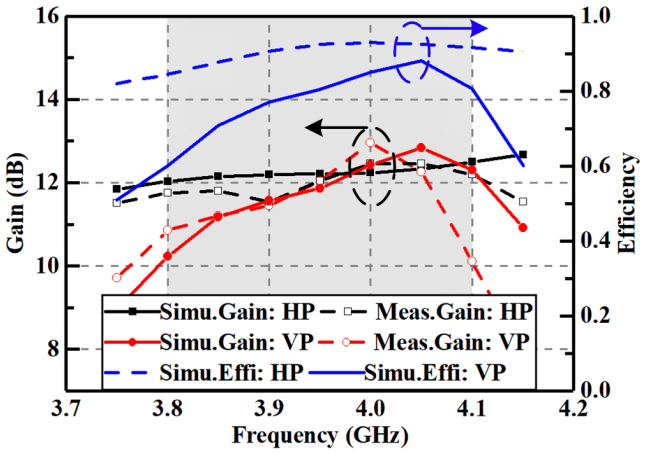

Fig. 14. Gains and efficiency of the proposed dual-linearly polarized antenna.

D. Gains and Total Efficiency

The comparison between simulated and measured endfire gains is illustrated in Fig. 14. It is seen that the measured results agree well with the simulated ones. The measured endfire gains of both the CRMS and the DSSAA are better than 10 dB from 3.8 to 4.1 GHz with the maximum values of 12.5 and 12.9 dB, respectively. The discrepancy is mainly caused by the soldering error and the foams loaded. Thanks to the all-metal strategy with negligible dielectric and metal loss, a high antenna efficiency better than 80% of the CRMS is realized as shown in Fig. 14. It is noted that the total efficiency of the DSSAA is related to the coupling level between the double-sided slots and the PSL. Hence, the simulated minimum and maximum efficiency of the DSSAA is 60.2% at 3.8 GHz and 88% at 4.05 GHz.

To highlight the novelty of the proposed design scheme, comparisons of the measured results between our work and other endfire antennas in the open literature were summarized in Table III. Table III indicates that most of the published works with endfire radiation are single polarization. The proposed antenna shows high endfire gain in two polarization states with acceptable electric size and bandwidth. Compared to the dual-polarized endfire works [31]–[33], the proposed antenna has smaller transverse dimensions. The effective radiation aperture in [32] is limited due to the partly radiated property of log-period dipole antennas. Compared with the Vivaldi antenna [33], a more uniform *E*-field distribution is achieved in this work. Hence, higher endfire gain is obtained in this work, though the log-period dipole antenna [32], Vivaldi antenna [33], and our work show similar electrical length.

V. CONCLUSION

In this work, a dual-linearly polarized antenna with high endfire gain and compact size is proposed. We employ the DSSAA and the CRMS to realize vertical and HP, respectively. Approximately uniform *E*-field amplitude distributions are obtained in two polarization states for high endfire gain. In pursuit of the compact size of the antenna, the top plate of

the DSSAA is also worked as the CRMS. To the best of our knowledge, no dual-linearly polarized endfire antennas with high gain and low profile have been published. The proposed design scheme offers a new solution to the dual-polarized endfire antennas with advantages of high gain, stable radiation patterns, and compact size.

REFERENCES

[1] S. Uda, "On the wireless beam of short electric waves," *J. Inst. Elec. Eng.*, vol. 452, pp. 273–282, Mar. 1926.

[2] H. Yagi, "Beam transmission of ultra short waves," *Proc. IRE*, vol. 16, no. 6, pp. 715–740, Jun. 1928.

[3] J. Shi, L. Zhu, N.-W. Liu, and W. Wu, "A microstrip Yagi antenna with an enlarged beam tilt angle via a slot-loaded patch reflector and pin-loaded patch directors," *IEEE Antennas Wireless Propag. Lett.*, vol. 18, no. 4, pp. 679–683, Apr. 2019.

[4] E. Guo, J. Liu, and Y. Long, "A mode-superposed microstrip patch antenna and its Yagi array with high front-to-back ratio," *IEEE Trans. Antennas Propag.*, vol. 65, no. 12, pp. 7328–7333, Dec. 2017.

[5] Z. Liang, J. Liu, Y. Zhang, and Y. Long, "A novel microstrip quasi Yagi array antenna with annular sector directors," *IEEE Trans. Antennas Propag.*, vol. 63, no. 10, pp. 4524–4529, Oct. 2015.

[6] Z. Yang, L. Zhang, and T. Yang, "A microstrip magnetic dipole Yagi–Uda antenna employing vertical I-shaped resonators as parasitic elements," *IEEE Trans. Antennas Propag.*, vol. 66, no. 8, pp. 3910–3917, Aug. 2018.

[7] J. Liu and Q. Xue, "Microstrip magnetic dipole Yagi array antenna with endfire radiation and vertical polarization," *IEEE Trans. Antennas Propag.*, vol. 61, no. 3, pp. 1140–1147, Mar. 2013.

[8] Z. Hu, Z. Shen, W. Wu, and J. Lu, "Low-profile top-hat monopole Yagi antenna for end-fire radiation," *IEEE Trans. Antennas Propag.*, vol. 63, no. 7, pp. 2851–2857, Jul. 2015.

[9] Z. Hu, Z. Shen, W. Wu, and J. Lu, "Low-profile log-periodic monopole array," *IEEE Trans. Antennas Propag.*, vol. 63, no. 12, pp. 5484–5491, Dec. 2015.

[10] G. Liu, H. Li, Y. Chen, H. He, S. Gao, and S. Yang, "A wideband, low-profile log-periodic monopole array with end-fire scanning beams," *IEEE Antennas Wireless Propag. Lett.*, vol. 17, no. 12, pp. 2414–2418, Dec. 2018.

[11] Q. Song, Z. Shen, and J. Lu, "Log-periodic monopole array with uniform spacing and uniform height," *IEEE Trans. Antennas Propag.*, vol. 66, no. 9, pp. 4687–4694, Sep. 2018.

[12] Q. Chen, Z. Hu, Z. Shen, and W. Wu, "2–18 GHz conformal low-profile log-periodic array on a cylindrical conductor," *IEEE Trans. Antennas Propag.*, vol. 66, no. 2, pp. 729–736, Feb. 2018.

[13] Z. Hu, S. Cao, M. Liu, C. Hua, and Z. Chen, "A planar low-profile log-periodic array based on cavity-backed slot," *IEEE Antennas Wireless Propag. Lett.*, vol. 18, no. 10, pp. 1966–1970, Oct. 2019.

[14] K. Anim and Y.-B. Jung, "Shortened log-periodic dipole antenna using printed dual-band dipole elements," *IEEE Trans. Antennas Propag.*, vol. 66, no. 12, pp. 6762–6771, Dec. 2018.

[15] H. Wang, K. E. Kedze, and I. Park, "A high-gain and wideband series-fed angled printed dipole array antenna," *IEEE Trans. Antennas Propag.*, vol. 68, no. 7, pp. 5708–5713, Jul. 2020.

[16] D. R. Jackson, C. Caloz, and T. Itoh, "Leaky-wave antennas," *Proc. IEEE*, vol. 100, no. 7, pp. 2194–2206, Jul. 2012.

[17] J. Liu, D. R. Jackson, and Y. Long, "Substrate integrated waveguide (SIW) leaky-wave antenna with transverse slots," *IEEE Trans. Antennas Propag.*, vol. 60, no. 1, pp. 20–29, Jan. 2012.

[18] J. Liu, D. R. Jackson, Y. Li, C. Zhang, and Y. Long, "Investigations of SIW leaky-wave antenna for endfire-radiation with narrow beam and sidelobe suppression," *IEEE Trans. Antennas Propag.*, vol. 62, no. 9, pp. 4489–4497, Sep. 2014.

[19] J. Liu, "Substrate integrated surface-wave antenna," *IEEE Trans. Antennas Propag.*, vol. 67, no. 8, pp. 5221–5230, Aug. 2019.

[20] P. Liu, H. Feng, Y. Li, and Z. Zhang, "Low-profile endfire leaky-wave antenna with air media," *IEEE Trans. Antennas Propag.*, vol. 66, no. 3, pp. 1086–1092, Mar. 2018.

[21] Y. Hou, Y. Li, Z. Zhang, and M. F. Iskander, "All-metal endfire antenna with high gain and stable radiation pattern for the platform-embedded application," *IEEE Trans. Antennas Propag.*, vol. 67, no. 2, pp. 730–737, Feb. 2019.

[22] L. Sun, Y. Hou, Y. Li, Z. Zhang, and Z. Feng, "An open cavity leaky-wave antenna with vertical-polarization endfire radiation," *IEEE Trans. Antennas Propag.*, vol. 67, no. 5, pp. 3455–3460, May 2019.

[23] Y. Hou, Y. Li, Z. Zhang, and Z. Feng, "Narrow-width periodic leaky-wave antenna array for endfire radiation based on Hansen–Woodyard condition," *IEEE Trans. Antennas Propag.*, vol. 66, no. 11, pp. 6393–6396, Nov. 2018.

[24] L. Sun, P. Liu, Y. Li, L. Chang, K. Wei, and Z. Zhang, "Metal strip endfire antenna based on TE_1 leaky-wave mode," *IEEE Trans. Antennas Propag.*, vol. 68, no. 8, pp. 5916–5923, Aug. 2020.

[25] A. Kandwal, Q. Zhang, X.-L. Tang, L. W. Liu, and G. Zhang, "Low-profile spoof surface plasmon polaritons traveling-wave antenna for near-endfire radiation," *IEEE Antennas Wireless Propag. Lett.*, vol. 17, no. 2, pp. 184–187, Feb. 2018.

[26] X. Du, H. Li, and Y. Yin, "Wideband fish-bone antenna utilizing odd-mode spoof surface plasmon polaritons for endfire radiation," *IEEE Trans. Antennas Propag.*, vol. 67, no. 7, pp. 4848–4853, Jul. 2019.

[27] W. Feng, Y. Feng, L.-S. Wu, Y. Shi, X. Y. Zhou, and W. Che, "A novel leaky wave endfire filtering antenna based on spoof surface plasmon polaritons," *IEEE Trans. Plasma Sci.*, vol. 48, no. 9, pp. 3061–3066, Sep. 2020.

[28] Y. Dong and T. Itoh, "Substrate integrated composite right-/left-handed leaky-wave structure for polarization-flexible antenna application," *IEEE Trans. Antennas Propag.*, vol. 60, no. 2, pp. 760–771, Feb. 2012.

[29] H.-W. Yu, Y.-C. Jiao, C. Zhang, and Z.-B. Weng, "Dual-linearly polarized leaky-wave patch array with low cross-polarization levels using symmetrical spoof surface plasmon polariton lines," *IEEE Trans. Antennas Propag.*, vol. 69, no. 3, pp. 1781–1786, Mar. 2021.

[30] Y.-H. Ren, J. Ding, C.-J. Guo, Y.-C. Song, and Y. Qu, "A wideband gain-enhanced dual-polarized printed antenna based on log-periodic parasitic directors (LPPDs)," *J. Electromagn. Waves Appl.*, vol. 30, no. 8, pp. 1021–1031, May 2016.

[31] O. Kramer, T. Djerafi, and K. Wu, "Vertically multilayer-stacked Yagi antenna with single and dual polarizations," *IEEE Trans. Antennas Propag.*, vol. 58, no. 4, pp. 1022–1030, Apr. 2010.

[32] H. Shirinabadi, M. Ahmadi-Boroujeni, E. Arbabi, and K. Mohammadpour-Aghdam, "Design of a printed non-planar dual-polarised log-periodic dipole array," *IET Microw., Antennas Propag.*, vol. 11, no. 4, pp. 490–494, Mar. 2017.

[33] M. Sonkki, D. Sanchez-Escuderos, V. Hovinen, E. T. Salonen, and M. Ferrando-Bataller, "Wideband dual-polarized cross-shaped Vivaldi antenna," *IEEE Trans. Antennas Propag.*, vol. 63, no. 6, pp. 2813–2819, Jun. 2015.

[34] Z. Shen and C. Feng, "A new dual-polarized broadband horn antenna," *IEEE Antennas Wireless Propag. Lett.*, vol. 4, pp. 270–273, 2005.

[35] C. A. Balanis, *Antenna Theory Analysis and Design*, 3rd ed. Hoboken, NJ, USA: Wiley, 2005.

[36] Ansoft Corp., Pittsburgh, PA, USA. *HFSS V15*. Accessed: May 1, 2021. [Online]. Available: http://www.ansys.com/products/electronics/ansys-hfss

[37] W. W. Hansen and J. R. Woodyard, "A new principle in directional antenna design," *Proc. IRE*, vol. 26, no. 3, pp. 333–345, Mar. 1938.

Weiquan Zhang received the B.S. degree from the University of Electronic Science and Technology of China, Chengdu, China, in 2018. He is currently pursuing the Ph.D. degree in electrical engineering with Tsinghua University, Beijing, China.

His current research interests include reconfigurable antennas, multimode antennas, and reflectarray antennas.

Yue Li (Senior Member, IEEE) received the B.S. degree in telecommunication engineering from Zhejiang University, Zhejiang, China, in 2007, and the Ph.D. degree in electronic engineering from Tsinghua University, Beijing, China, in 2012.

He is currently an Associate Professor with the Department of Electronic Engineering, Tsinghua University. In June 2012, he joined the Department of Electronic Engineering, Tsinghua University, as a Post-Doctoral Fellow. In December 2013, he joined the Department of Electrical and Systems Engineering, University of Pennsylvania, Philadelphia, PA, USA, as a Research Scholar. He was also a Visiting Scholar with the Institute for Infocomm Research (I2R), A∗STAR, Singapore, in 2010, and the Hawaii Center of Advanced Communication (HCAC), University of Hawaii at Manoa, Honolulu, HI, USA, in 2012. Since January 2016, he has been with Tsinghua University, where he is currently an Assistant Professor. He has authored or coauthored over 160 journal articles and 50 international conference papers, and holds 24 granted Chinese patents. His current research interests include metamaterials, plasmonics, electromagnetics, nanocircuits, mobile and handset antennas, MIMO and diversity antennas, and millimeter-wave antennas and arrays.

Dr. Li was a recipient of the Issac Koga Gold Medal from URSI General Assembly in 2017; the Second Prize of Science and Technology Award of China Institute of Communications in 2017; the Young Scientist Awards from the conferences of PIERS 2019, ACES 2018, AT-RASC 2018, AP-RASC 2016, EMTS 2016, and URSI GASS 2014; the Best Paper Awards from the conferences of APCAP 2020/2017, UCMMT 2020, ISAP 2019, CSQRWC 2018, NCMMW 2018/2017, NCANT 2019/2017, ISAPE 2016, and ICMMT 2020/2016; the Outstanding Doctoral Dissertation of Beijing Municipality in 2013, and the Principal Scholarship of Tsinghua University in 2011. He is serving as the Associate Editor of the IEEE TRANSACTIONS ON ANTENNAS AND PROPAGATION, the IEEE ANTENNAS AND WIRELESS PROPAGATION LETTERS, the *Microwave and Optical Technology Letters*, and the *Computer Applications in Engineering Education*, and also as the Editorial Board of *Scientific Report and Electronics*.

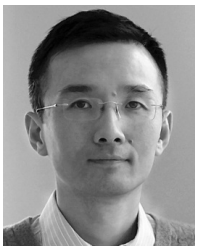

Zhijun Zhang (Fellow, IEEE) received the B.S. and M.S. degrees from the University of Electronic Science and Technology of China, Chengdu, China, in 1992 and 1995, respectively, and the Ph.D. degree from Tsinghua University, Beijing, China, in 1999.

In 1999, he joined the Department of Electrical Engineering, University of Utah, Utah, U.K., as a Post-Doctoral Fellow, where he was appointed a Research Assistant Professor in 2001. In May 2002, he joined the University of Hawaii at Manoa, Honolulu, HI, USA, as an Assistant Researcher. In November 2002, he joined Amphenol T&M Antennas, Vernon Hills, IL, USA, as a Senior Staff Antenna Development Engineer and was then promoted to the position of Antenna Engineer Manager. In 2004, he joined Nokia, Inc., San Diego, CA, USA, as a Senior Antenna Design Engineer. In 2006, he joined Apple, Inc., Cupertino, CA, as a Senior Antenna Design Engineer and was then promoted to the position of Principal Antenna Engineer. Since August 2007, he has been with Tsinghua University, where he is currently a Professor with the Department of Electronic Engineering. He has authored the *Antenna Design for Mobile Devices* (Wiley, 1st ed. 2011, 2nd ed. 2017).

Dr. Zhang served as an Associate Editor of the IEEE TRANSACTIONS ON ANTENNAS AND PROPAGATION from 2010 to 2014 and the IEEE ANTENNAS AND WIRELESS PROPAGATION LETTERS from 2009 to 2015.